International Journal of Thermophysics, Vol. 27, No. 1, January 2006 (© 2006)
DOI: 10.1007/s10765-006-0037-2

Estimation of Thermal Contact Resistance Using Ultrasonic Waves[1]

P. Z. Cong,[2] X. Zhang,[3,4] and M. Fujii[3]

In this paper, numerical simulations of both the three-dimensional heat conduction and two-dimensional elastic wave propagation at the interface of contact solids have been carried out. Numerical results of heat conduction simulations show that both the true contact area and thermal contact conductance increase linearly with an increase in the contact pressure. Numerical results of the ultrasonic wave propagation show that the intensity of a transmitted wave is very weak but depends clearly on the contact pressure. On the other hand, the intensity of reflected wave amounts to more than 99% of the standard reflected wave that results from the case of one cylindrical specimen without contact. However, the intensity of the modified reflected wave defined by the difference between the reflected wave and standard reflected wave shows the same tendency as that of the transmitted wave. The intensities of both transmitted and modified reflected waves could be expressed by the same power function of the contact pressure. By comparing the results of heat conduction with those of ultrasonic propagation calculations, a power functional correlation between the thermal contact conductance and transmitted or modified reflected intensity has been obtained. Using this correlation, it will be possible to estimate the thermal contact conductance between two solids through measuring the intensity of either reflected or transmitted ultrasonic waves.

KEY WORDS: nondestructive measurement; numerical simulation; thermal contact conductance; thermal contact resistance; ultrasonic wave.

[1] Paper presented at the Seventh Asian Thermophysical Properties Conference, August 23–28, 2004, Hefei and Huangshan, Anhui, P. R. China.

[2] Interdisciplinary Graduate School of Engineering Sciences, Kyushu University, Kasuga 816-8580, Japan.

[3] Institute for Materials Chemistry and Engineering, Kyushu University, Kasuga 816-8580, Japan.

[4] To whom correspondence should be addressed. E-mail: xzhang@cm.kyushu-u.ac.jp

1. INTRODUCTION

The thermal contact resistance (TCR) is an important issue for thermal designers of electronic devices as it is directly related to the cooling performance of central processing units (CPUs) [1]. Although many theoretical and empirical correlations have been developed for predicting the TCR in the past five decades [2], it is still difficult to know an exact value in an actual case where the contact pressure is generally unknown. Therefore, it is desirable to develop an *in situ* diagnostic method to estimate the TCR. Since ultrasonic waves can be applied to metallic, non-metallic, transparent and opaque materials, an ultrasonic technique is considered to be one of the candidates for *in situ* and nondestructive measurements of the TCR. Kendall and Tabor [3] conducted theoretical and experimental studies to determine quantitatively the true contact area at the interface of stationary and sliding contacts by means of an ultrasonic technique. Alterman and Loewenthal [4] described how to use finite difference methods to obtain complete theoretical seismograms for a source in a layered half-space, in wedges, and in a sphere. Tomimura et al. [5] reported a method to estimate the thermal contact conductance (TCC) of metals by measuring ultrasonic transmitted waves. Fujii et al. [6] further studied numerically ultrasound propagation through a solid-solid interface.

In the present paper, we will report how to use reflected and transmitted ultrasonic intensities to estimate the thermal contact resistance or thermal contact conductance (TCC = 1/TCR) for two end-contacted cylindrical specimens with a random roughness at the contact interface. Numerical simulations have been done to clarify the effects of the contact pressure on the intensities of reflected and transmitted ultrasonic waves and on both the true contact area and TCC. A functional correlation between the TCC and the transmitted and reflected intensities has been presented. Further, by using this correlation, an *in situ* and nondestructive method for measurement of the TCR or TCC is proposed through measuring either the intensity of modified reflected or transmitted ultrasonic waves.

2. CALCULATIONS

2.1. Heat Conduction

Figure 1 shows the physical model and coordinate system. A pair of cylindrical specimens of height H and diameter D is pressed together with an equivalent mean nominal contact pressure p. Specimens I and II have thermal conductivities k_{I} and k_{II}, and maximum roughness heights $R_{\max \mathrm{I}}$ and $R_{\max \mathrm{II}}$, respectively. For the heat conduction simulations a uniform

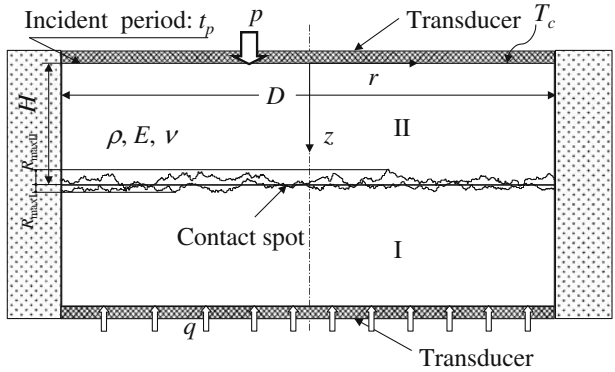

Fig. 1. Physical model.

heat flux is supplied at the bottom surface of the lower specimen, a uniform temperature is assumed at the top surface of the upper specimen, and the peripheral surfaces of the two specimens are thermally insulated.

The dimensionless surface roughness, $Z_s(R,\theta)$, is constructed with a random number surface model as expressed by

$$Z_s(R,\theta) = B\sum_{i=1}^{n} \sin\left[\frac{2\pi R\cos(\theta+\alpha_i)}{L_i} - \varphi_i\right] \tag{1}$$

where R and θ are the dimensionless radius and angle in cylindrical coordinates, L_i is the dimensionless wavelength, and B is the dimensionless scale factor. These are defined as

$$R = \frac{r}{R_a},\quad L_i = \frac{l_i}{R_a},\quad B = \frac{\pi R_0^2}{\int_0^{2\pi}\int_0^{R_0}\left|\sum_{i=1}^{n}\left[\frac{2\pi R\cos(\theta+\alpha_i)}{L_i} - \varphi_i\right]\right| R\,dR\,d\theta} \tag{2}$$

where R_a is the mean surface roughness, R_0 is the dimensionless radius of specimen, n is the upper limit number of superposed waves used to construct the surface, and l_i, φ_i, and α_i are the wavelength, initial phase and orientation at the number i of superposed waves. When two surfaces with similar roughness expressed by Eq. (1) come into contact and are pressurized, each asperity of roughness is assumed to be deformed under fully plastic conditions.

The equiperipheral grid system as shown in Fig. 2 has been developed and used to obtain a real contact spot distribution as shown in Fig. 3, and also to solve the three-dimensional heat conduction. A new network method

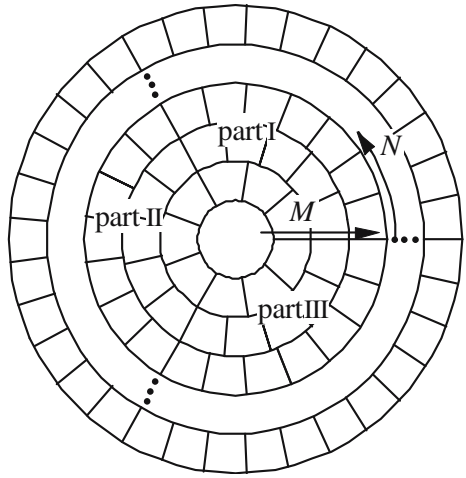

Fig. 2. Equiperipheral grid system.

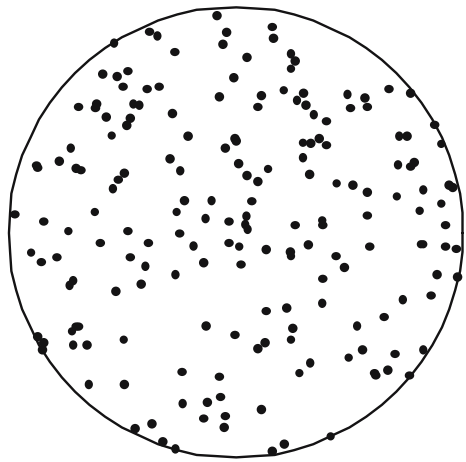

Fig. 3. Distribution of contact spots.

[7] based on the equiperipheral grid system is applied for the heat conduction calculation. Figure 4 shows a typical network of the equiperipheral grid system in the r-θ plane. To calculate the heat flows across the control surfaces perpendicular to the radial direction, the interpolated temperatures are used at the fictitious nodes 1 and 4 adjacent to the control volume 0. The temperatures at the peripherally adjacent nodes 2 and 3 are directly used to calculate the heat flows across the related control surfaces. In the present calculations, 80 grids in the radial direction are used to obtain the numerical results that are independent of the number of grids [7].

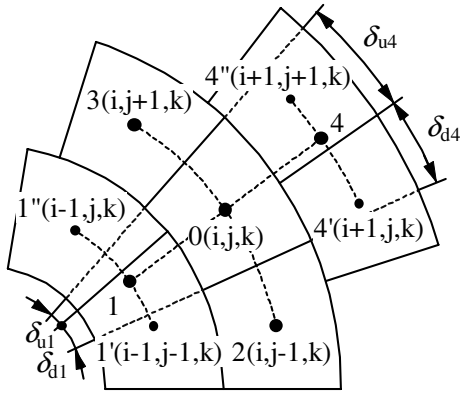

Fig. 4. Equiperipheral grids.

2.2. Ultrasound Propagation

Based on the physical model shown in Fig. 1, two transducers with the same diameter as the specimens are attached to the bottom and top surfaces of the specimens. The incident wave is radiated from the top surface. Therefore, the upper transducer receives the reflected signal and the lower one receives the transmitted signal. The dimensionless equations of elastic wave motion in R-Z plane are expressed by

$$\Phi \frac{\partial^2 U}{\partial \tau^2} = (\Lambda + 2\mathrm{M}) \frac{\partial \Gamma}{\partial R} + \mathrm{M} \frac{\partial \Omega_\theta}{\partial Z} \tag{3}$$

$$\Phi \frac{\partial^2 W}{\partial \tau^2} = (\Lambda + 2\mathrm{M}) \frac{\partial \Gamma}{\partial Z} - \frac{\mathrm{M}}{R} \frac{\partial (R\Omega_\theta)}{\partial R} \tag{4}$$

$$\Gamma = \frac{\partial U}{\partial R} + \frac{U}{R} + \frac{\partial W}{\partial Z}, \quad \Omega_\theta = \frac{\partial U}{\partial Z} - \frac{\partial W}{\partial R} \tag{5}$$

where R and Z are the dimensionless cylindrical coordinates, U and W are the dimensionless displacements in R- and Z-directions, respectively, and τ is the dimensionless time. These dimensionless variables are defined by

$$U = \frac{u}{D}, \qquad W = \frac{w}{D}, \qquad \tau = \frac{t}{t_p}, \qquad R = \frac{r}{D}, \qquad Z = \frac{z}{D} \tag{6}$$

where r and z are the coordinates, u and w are the displacements in r- and z-directions, t is time, and t_p is the duration of pulse. The

dimensionless density, Φ, and dimensionless Lamé constants, Λ and M, are further defined by

$$\Phi = \frac{D^2\rho}{t_p^2 E}, \qquad \Lambda = \frac{\lambda}{E}, \qquad \mathrm{M} = \frac{\mu}{E} \tag{7}$$

where ρ is the density, E is Young's modulus, and λ and μ are Lamé constants.

The initial boundary conditions describe the free of strain conditions and the incidence of ultrasound radiation, and are expressed by

$$\Lambda \frac{U}{R} + \Lambda \frac{\partial U}{\partial R} + (\Lambda + 2\mathrm{M}) \frac{\partial W}{\partial Z} = -F(\tau) \tag{8}$$

$$\sigma_{rz} = \sigma_{zr} = \mathrm{M}\left(\frac{\partial U}{\partial Z} + \frac{\partial W}{\partial R}\right) = 0 \tag{9}$$

where σ_{rz} and σ_{zr} are the shearing stresses in the r- and z-directions, $F(\tau)$ is the dimensionless source function of the pulse pressure supplied to the top surface and defined by

$$F(\tau) = \begin{cases} P_s \sin^2(2\pi\tau) & (0 \leqslant \tau \leqslant 1) \\ 0 & (\tau > 1) \end{cases} \tag{10}$$

Here, P_s is the dimensionless amplitude of source function.

The free boundary conditions applied for the noncontact interface, that is, the gap and peripheral surface, are expressed by

$$\sigma_{zz} = \Lambda \frac{U}{R} + \Lambda \frac{\partial U}{\partial R} + (\Lambda + 2\mathrm{M}) \frac{\partial W}{\partial Z} = 0 \tag{11}$$

$$\sigma_{rr} = \Lambda \frac{U}{R} + \Lambda \frac{\partial W}{\partial Z} + (\Lambda + 2\mathrm{M}) \frac{\partial U}{\partial R} = 0 \tag{12}$$

where σ_{zz} and σ_{rr} are the normal stresses in the z- and r-directions.

The conditions of continuity of stresses and displacements are set at the real contact spots. These are expressed by

$$\sigma_{zz} = (\Lambda + 2\mathrm{M}) \frac{\partial W^I}{\partial Z} + \Lambda \frac{\partial U^I}{\partial R} = (\Lambda + 2\mathrm{M}) \frac{\partial W^{II}}{\partial Z} + \Lambda \frac{\partial U^{II}}{\partial R} \tag{13}$$

$$\sigma_{zr} = \mathrm{M}\left(\frac{\partial U^I}{\partial Z} + \frac{\partial W^I}{\partial R}\right) = \mathrm{M}\left(\frac{\partial U^{II}}{\partial Z} + \frac{\partial W^{II}}{\partial R}\right) \tag{14}$$

$$W^I = W^{II}, \qquad U^I = U^{II} \tag{15}$$

Finite difference formulations [4] were used to separate the elastic differential equations of motion described above. Stability conditions given by Alterman and Loewenthal [4] were used in the present calculations. Since two specimens are assumed to be the same materials, the ultrasonic wave at the contact spots is perfectly transmitted, but the wave is reflected perfectly at a gap due to the large difference of acoustic impedance between air and the solid specimen. In the present calculations, a 601 by 1001 grid is used in the R- and Z-directions, respectively. The present results agree well with those obtained numerically by Hatano et al. [8].

3. RESULTS AND DISCUSSION

Figure 5 shows the time evolution of strain observed at the top surface for a single cylindrical specimen without contact. In this case, the ultrasonic wave is perfectly reflected at the end surface. The incident wave is observed within $\tau = 1$, while the first reflected wave is observed at $\tau = 6.9$ to 7.9. In the present paper, this reflected wave is designated as the standard reflected wave (SRW).

Figure 6 shows the relationship between the true contact area A obtained by assuming the specimens to be fully plastic and contact pressure $P(P = p/E)$. The true contact area increases linearly with an increase in the contact pressure. Figure 7 shows the relation between the calculated TCC, that is, $H_m(H_m = h_m R_a/k)$ and the contact pressure. It is clear that

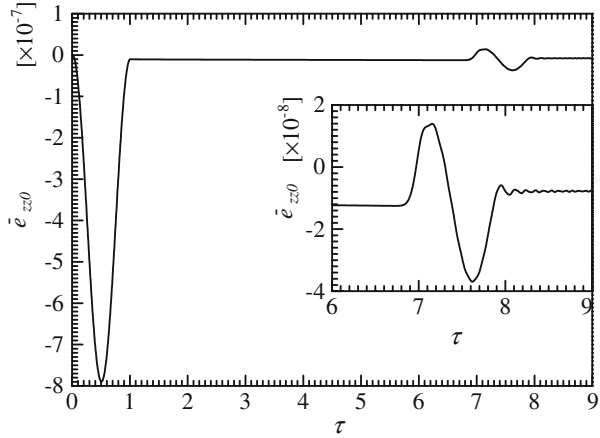

Fig. 5. Strain of reflected wave for one cylindrical specimen.

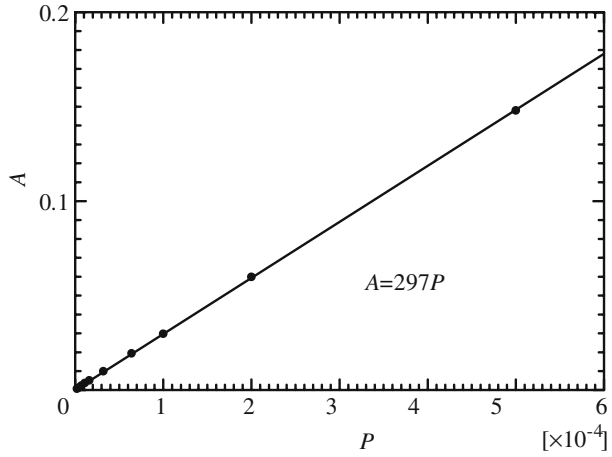

Fig. 6. Relation between true contact area and contact pressure.

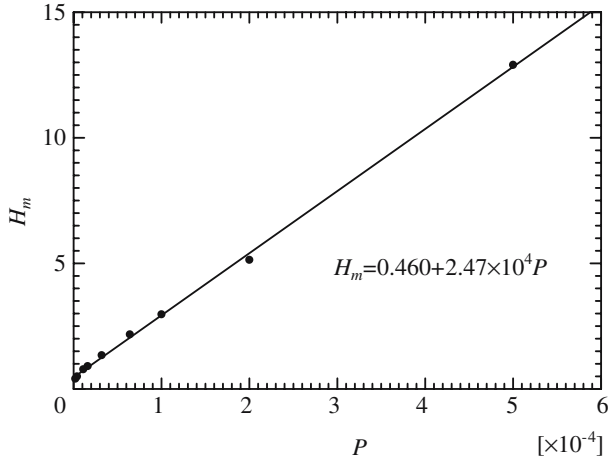

Fig. 7. Relation between H_m and P.

H_m also increases linearly with the contact pressure P. At a lower contact pressure, the true contact area is less than 1% of the total area of the interface. Therefore, the strain difference between the reflected wave and SRW is also expected to be less than 1% of the strain caused by SRW. To make this difference clear, the modified strain, Δ, is defined as the difference between the strain of the reflected wave and the standard reflected wave by

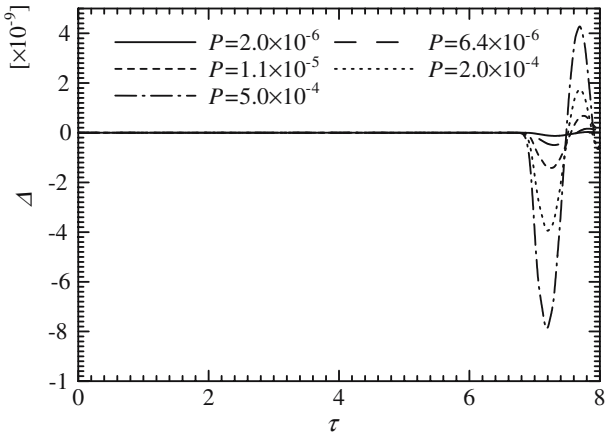

Fig. 8. Difference of strain of reflected wave.

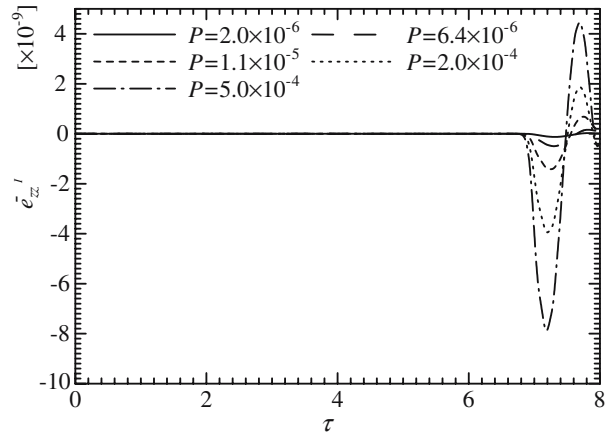

Fig. 9. Strain of transmitted wave.

$$\text{Difference of strain:} \Delta = \bar{e}_{zz}^{II} - \bar{e}_{zz0} \tag{16}$$

Here, $\bar{e}_{zz0}$ is the area averaged strain of SRW and $\bar{e}_{zz}^{II}$ is the average strain of the reflected wave observed at the top surface. Figure 8 shows the time evolution of the modified strain at the top surface. The modified strain is clearly shown to be dependent on the contact pressure.

Figure 9 shows the strain of transmitted wave, $\bar{e}_{zz}^{I}$ observed at the bottom surface. As expected, the modified strain and the strain of the transmitted wave are almost equal, which means that the energy balance

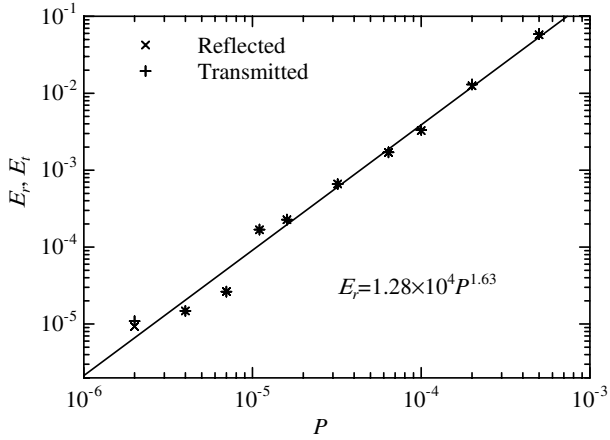

Fig. 10. Relation between E_r, E_t and contact pressure.

is reasonable in the present calculations. Consequently, both of the strains at the top and bottom surfaces increase with an increase of the contact pressure.

In order to show the relationship between the strains and contact pressure, the normalized strains E_r and E_t, are introduced that are defined as the ratios of intensity of modified strain and that of transmitted wave, respectively, to the intensity of SRW and expressed by

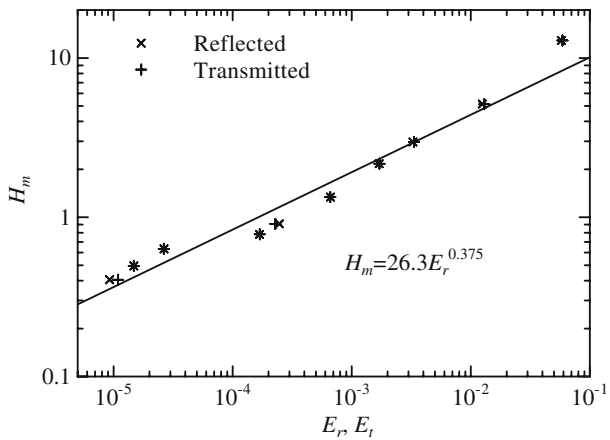

Fig. 11. Relation between H_m and E_r, E_t.

$$E_r = \frac{(\Delta)^2}{(\bar{e}_{zz0})^2}; \qquad E_t = \frac{\left(\bar{e}^I_{zz}\right)^2}{(\bar{e}_{zz0})^2} \tag{17}$$

Based on the definition described above, the relation between these normalized intensities and contact pressure is obtained and shown in Fig. 10. It is clear that both intensities can be expressed by the same power functional correlation with the contact pressure.

By comparing the results of E_r, E_t and contact pressure with that of TCC and P, a power functional correlation between H_m and intensities E_r or E_t is obtained and shown in Fig. 11. Using this correlation, it is possible to estimate the TCC between two solids though measuring either the intensity of a reflected or transmitted ultrasonic wave.

4. CONCLUSIONS

Numerical simulations have been performed on heat conduction and ultrasonic propagation through a solid-solid contact interface. The main conclusions are as follows:

(a) The true contact area and thermal contact conductance are linearly proportional to the contact pressure in the present pressure range.

(b) There is a power functional relation between the thermal contact conductance and both the transmitted and reflected ultrasonic intensities.

(c) It is possible to estimate the thermal contact conductance by measuring either the intensity of reflected or transmitted ultrasonic waves.

NOMENCLATURE

A	dimensionless true contact area
B	dimensionless scale factor
D	diameter of specimen (m)
E	Young's modulus (Pa)
$\bar{e}_{zz}$	dimensionless area averaged strain in Z-direction
H	height of specimen (m)
H_m	dimensionless thermal contact conductance
k	thermal conductivity of specimen
L_i	dimensionless wavelength of surface roughness
l_i	wavelength of surface roughness (m)
M	grid number in radial direction

N	grid number in peripheral direction
n	upper limit number of superposed waves
P	dimensionless mean nominal contact pressure
p	mean nominal contact pressure (Pa)
P_s	dimensionless amplitude of source function
q	heat flux ($W \cdot m^{-2}$)
R	dimensionless radius in cylindrical coordinates
r	radius in cylindrical coordinates (m)
R_0	dimensionless radius of specimen
R_a	mean roughness (m)
RND	random number
$R_{\max}$	maximum roughness (m)
t	time (s)
T_c	temperature at the top surface (K)
t_p	duration of pulse (s)
U	dimensionless displacement in R-direction
u	displacement in r-direction (m)
W	dimensionless displacement in Z-direction
w	displacement in z-direction (m)
Z	dimensionless axis in cylindrical coordinates
z	axis in cylindrical coordinates
$Z_s(R, \theta)$	dimensionless height of surface roughness
α_i	orientation
Δ	difference between the strain of reflected wave and SRW
E_r, E_t	ratios of intensities of transmitted and modified reflected to the intensity of SRW
θ	angle in cylindrical coordinates
Λ, M	dimensionless lamé constants
λ, μ	Lamé constants (Pa)
σ_{rr}	normal stress in the r-direction
σ_{rz}	shearing stress in the r-direction
$\sigma_{z,r}$	shearing stress in the z-direction
$\sigma_{z,z}$	normal stress in the z-direction
τ	dimensionless time
ρ	density of specimens ($kg \cdot m^{-3}$)
Φ	dimensionless density of specimen
φ_i	initial phase

Subscripts

0	standard reflected wave
I	specimen I
II	specimen II
i	number
min	minimum

max	maximum
r	reflected wave
t	transmitted wave

REFERENCES

1. V. Sartre and M. Lallemand, *Appl. Therm. Eng*. **21**:221 (2001).
2. M. G. Cooper, B. B. Mikic, and M. M. Yovanovich, *Int. J. Heat Mass Transfer* **12**:279 (1969).
3. K. Kendall and D. Tabor, *Proc. R. Soc. London, Ser. A* **323**:321 (1971).
4. Z. Alterman and D. Loewenthal, in *Methods in Computational Physics* (Academic Press, New York and London, 1972), pp. 36–43.
5. T. Tomimura, T. Kurozumi, X. Zhang, and M. Fujii, *Proceedings of 33rd National Heat Transfer Symposium of Japan* **I**:159 (1996).
6. M. Fujii, Y. Matsuda, X. Zhang, and M. Tomimura, *Proceedings of 38th National Heat Transfer Symposium of Japan* **III**, 771 (2001).
7. X. Zhang, P. Z. Cong, S. Fujiwara, and M. Fujii, *Int. J. Heat Mass Transfer* **47**:1091 (2004).
8. H. Hatano, F. Hoki, and O. Matsuda, *Acoustic Soc. Jpn*. **51**:755 (1995).